JCTC Journal of Chemical Theory and Computation

Article

pubs.acs.org/JCTC

Gas-Phase Chemical Dynamics Simulations on the Bifurcating Pathway of the Pimaradienyl Cation Rearrangement: Role of Enzymatic Steering in Abietic Acid Biosynthesis

Matthew R. Siebert,[†] Paranjothy Manikandan,[†] Rui Sun,[†] Dean J. Tantillo,[‡] and William L. Hase*[,†]

[†]Department of Chemistry and Biochemistry, Texas Tech University, Lubbock, Texas 79409, United States

[‡]Department of Chemistry, University of California—Davis, Davis, California 95616, United States

Supporting Information

ABSTRACT: The biosynthesis of abietadiene is the first biosynthetically relevant process shown to involve a potential energy surface with a bifurcating reaction pathway. Herein, we use gas-phase, enzyme-free direct dynamics simulations to study the behavior of the key reaction (bifurcating) step, which is conversion of the C_{20} pimaradienyl cation to the abietadienyl cation. In a previous study (*J. Am. Chem. Soc.* **2011**, *133*, 8335), a truncated C_{10} model was used to investigate this reaction. The current work finds that the complete C_{20} pimaradienyl cation gives reaction dynamics similar to that reported for the truncated C_{10} model. We find that in the absence of the enzyme, the C_{20} abietadienyl cation is generated in almost equal quantity (1.3:1) as an unobserved (in nature) seven-membered ring product. These simulations allude to a need for abietadiene synthase to steer the reaction to avoid generation of the seven-membered ring product. The methodology of post-transition state chemical dynamics simulations is also considered. The trajectories are initiated at the rate-controlling transition state (TS) separating the pimaradienyl and abietadienyl cations. Accurate results are expected for the short-time direct motion from this TS toward the abietadienyl cation. However, the dynamics may be less accurate for describing the unimolecular reactions that occur in moving toward the pimaradienyl cation, due to the unphysical flow of zero-point energy.

INTRODUCTION

In the chemical literature, "bifurcate", which has a literal meaning "to cut in two", is often associated with potential energy surfaces (PESs).[1−8] Figure 1 shows an example PES exhibiting a pathway bifurcation. For this example, it is possible to analytically solve for the critical points. Stationary points in the x dimension are located on this surface by solving $\partial f/\partial x = 0$. First, one must realize that these two stationary points are saddle points (i.e., transition state structures, TSs), and second, these points are directly connected with no intervening minimum. On a surface without a pathway bifurcation, the progression from reactant to TS to product occurs completely along a valley. The bifurcating pathway displayed in Figure 1 differs from this case, since after the first TS a valley-ridge inflection (VRI) occurs. The VRI point may be located on this example surface by solving $\partial^2 f/\partial x^2 = 0$. Note that for higher dimensional, chemically interesting PESs, locating the VRI is nontrivial.[7,9,10]

Many reported pathway bifurcations link products that are symmetry related. In fact, any time symmetry is lost during the course of a chemical reaction, there must be a pathway bifurcation.[11] Scheme 1 shows a few of such cases,[2] including (1) H-atom transfer in the methoxyl radical;[12−18] (2) the conversion of cyclooctatetraene to semibulvalene;[19] and (3) double bond isomerization in cyclooctatetraene.[20−22] What garners increased interest are those PES pathway bifurcations that lead to chemically distinct products. Scheme 2 shows just two of these cases.[2,23−26]

When considering two products formed from the same starting material, the established model for determining the ratio of the two products is transition state theory (TST). However, in the case of a bifurcating pathway, TST fails—it provides a single rate constant for the formation of BOTH products. For this reason, standard quantum chemical methods, although able to plot out the minimum energy pathway and find such bifurcating pathways, are unable to provide information about the ratio of the final products expected to be generated experimentally. Chemical dynamics simulations are necessary for this.[1−7]

To the best of our knowledge, only one pathway bifurcation has been found with biosynthetic relevance, i.e., part of a carbocation rearrangement proposed to occur during the biosynthesis of abietic acid. Abietic acid (see below) is the diterpenoid present in tall oil (aka pine resin) mainly responsible for its polymerizable nature.[27] In nature, pine resin acts as a defense against physical injury. If the injury comes in the form of an insect attack, such as one launched by the bark beetle, low molecular weight mono- (C_{10}) and sesquiterpenoids (C_{15}) may act as toxins to the insects and their symbiots. Furthermore, these low molecular weight terpenoids act as solvents to mobilize diterpenoids to the wound site.[27] Once there, volatilization of the mono- and sesquiterpenoids results in concentration and oxidative polymerization of the diterpenoids, effectively sealing wounds and preventing further damage to the majestic trees.[27] Tall oil is not only of use to trees such as *Abies grandis* but is also collected as a byproduct of the paper industry (although some companies harvest it from

Received: January 20, 2012
Published: March 19, 2012

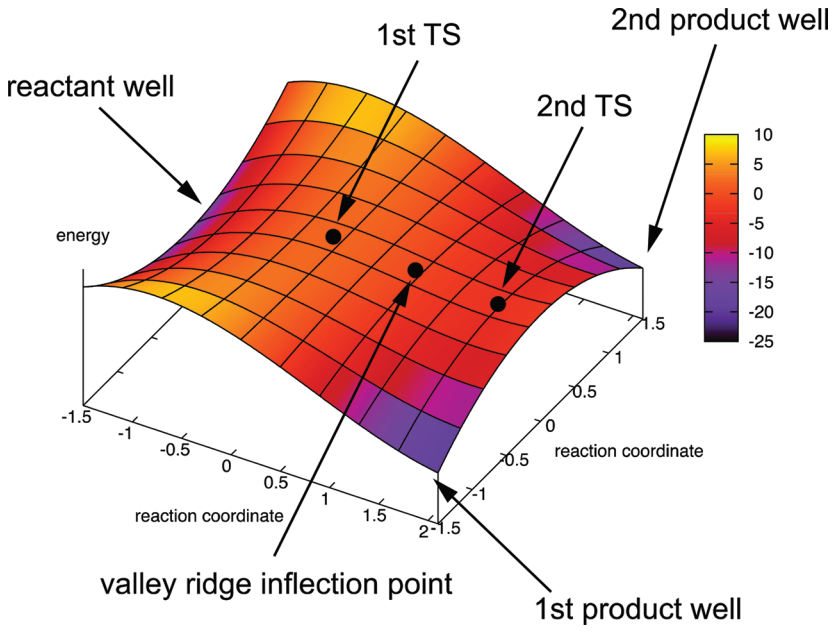

Figure 1. An example PES exhibiting a pathway bifurcation. Surface details: $f(x,y) = 2x^3 - 5x^2 - 5xy^2 + y^2 + 2$. Saddle points ($\partial f/\partial x = 0$) are located at (0, 0, 2) and (5/3, 0, −71/27); the valley ridge inflection point ($\partial^2 f/\partial x^2 = 0$) is located at (5/6, 0, −17/54).

Scheme 1. Example Bifurcating Pathways That Form Symmetry Related Products,[2] Including H-Atom Transfer in the Methoxyl Radical (top),[12−18] Conversion of Cyclooctatetraene to Semibulvalene (middle),[19] and Double Bond Isomerization in Cyclooctatetraene (bottom)[20−22]

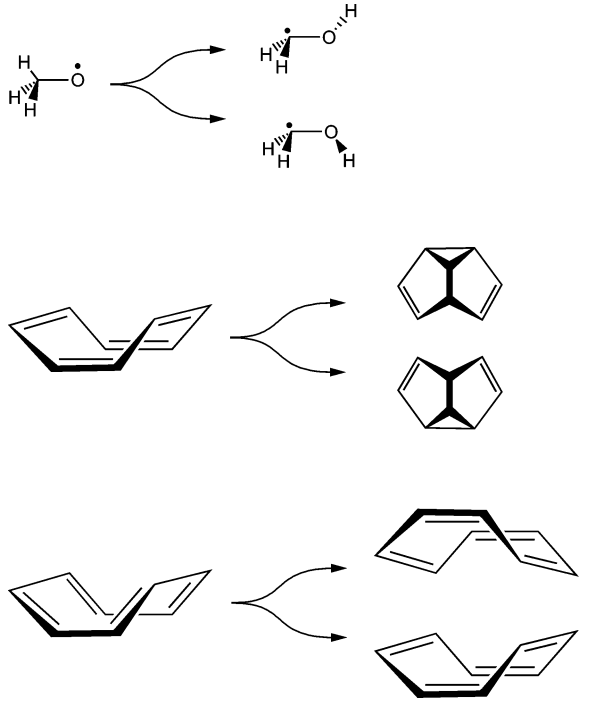

Scheme 2. Example Bifurcating Pathways That Form Chemically Unique Products[2,23−26]

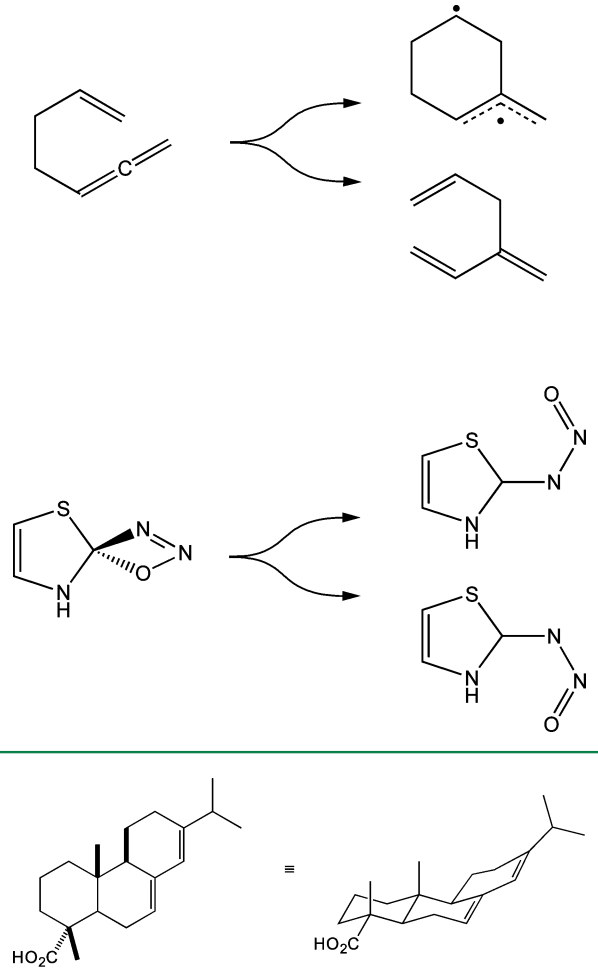

living trees) and is traded on the global market for its myriad uses in products including inks, adhesives, paper sizing, and chewing gum base.[28]

In 2009, Hong and Tantillo reported that the step converting the pimaradienyl cation to the abietadienyl cation occurs via a pathway bifurcation (see Scheme 3).[8] What is more, this bifurcation links the natural abietadienyl cation with a seven-membered ring cation whose deprotonation or trapping with

dx.doi.org/10.1021/ct300037p | J. Chem. Theory Comput. 2012, 8, 1212−1222

Scheme 3. Detailed Mechanism for the Conversion of Pimaradienyl Cation (1) to Abietadienyl Cation (4)

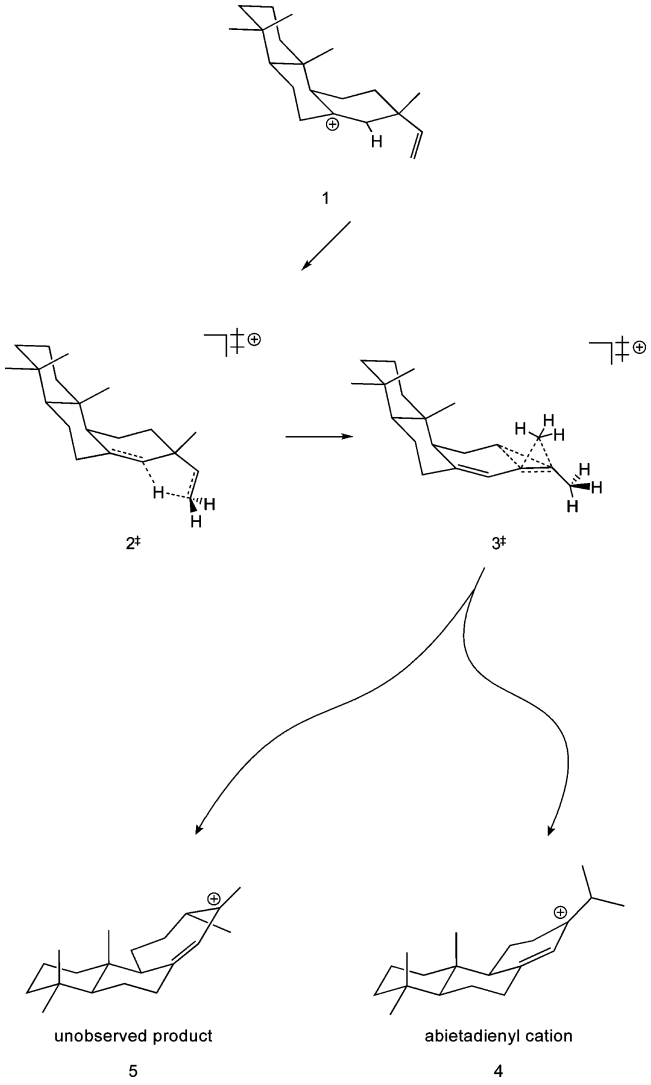

water would produce heretofore unobserved natural products. Previously, we reported on the gas-phase chemical dynamics simulations of a truncated C_{10} pimaradienyl cation → abietadienyl cation system (see Scheme 4).[1] We found a **4′**/**5′** ratio of 1.6:1, indicating that (at least in the absence of an enzyme template) a substantial fraction of **5′**, whose C_{20} congener is not observed naturally in the enzyme catalyzed process, would be expected to form. We put forth that this necessitates enzyme intervention to avoid forming detectable quantities of products derived from **5**. Herein, we extend this earlier study to the full C_{20} system, in the hopes of isolating any spurious results due to truncation of the natural system.

Scheme 4. Gas-Phase Chemical Dynamics Simulations (In the Absence of Abietadiene Synthase) for the Truncated C_{10} Model Predict a Ratio of 1.6:1 for 4′/5′

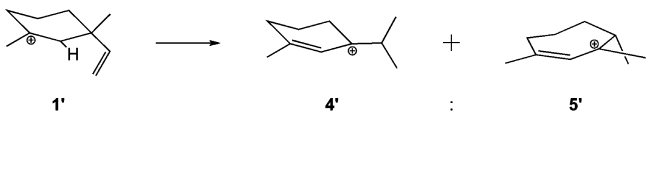

METHODS

Electronic Structure Calculations and Model for the PES. Electronic structure calculations were performed with the NWChem[29,30] computer program. The B3LYP/6-31G(d)[31−34] model chemistry was employed. Stationary points were classified as minima or TS structures by frequency analysis. Relative classical potential energies, without zero-point energy (ZPE) corrections, of the stationary points for the pimaradienyl cation rearrangement are listed in Table 1. Given in parentheses are the relative energies with ZPE corrections scaled by 0.9806.[35]

Table 1. Relative Potential Energies for Stationary Points on the PES for the Pimaradienyl Cation Rearrangement[a]

stationary point[b]	V [kcal/mol]
1	0.00 (*0.00*)
2‡	34.00 (*30.97*)
3‡	13.66 (*12.58*)
4	−28.11 (*-27.55*)
5	−17.24 (*-15.92*)
6	−14.74 (*-14.00*)

[a]Relative energies are B3LYP/6-31G(d) classical potential energies, without ZPE (normal text) and with scaled ZPE (*underlined italics*). [b]The stationary points are identified in Scheme 3 and Figure 2.

In our dynamics study on the truncated C_{10} system, we showed that the B3LYP/6-31+G(d,p) model chemistry produces reasonable results,[1] despite the myriad shortcomings identified with this particular density functional method.[36−48] It is well documented that B3LYP scales as N^4 where N equals the number of basis functions.[49] Given that a single trajectory simulation on the C_{10} system took one week of computer time (using eight cores), we expect that *each* C_{20} *trajectory* (double the basis functions) would take 16 times (2^4) as long, i.e., 16 weeks on eight cores of a dual 2.66 GHz Xeon E5430 quad-core node. For this reason, we aimed to reduce the computational time while preserving the qualitative accuracy. The slightly smaller 6-31G(d) basis set was employed, and as a test of its validity a small subset of trajectories was computed for the truncated C_{10} system, to compare with our previously published results.[1] The key details appear in Table 2.

Table 2. Product Distribution As a Function of Basis Set Size [6-31+G(d,p) vs 6-31G(d)]

	6-31+G(d,p)[a]	6-31G(d)[b]
4′	59 ± 5.0%	46 ± 7.2%
5′	35 ± 4.9%	42 ± 7.1%
cyclopropanation	5 ± 2.3%	13 ± 4.8%
ethylene elimination	1 ± 1.1%	0%

[a]100 total trajectories, five recross the barrier; data taken from ref 1. [b]50 total trajectories, two recross the barrier.

It is clear from Table 2 that the smaller 6-31G(d) basis set favors the formation of **5′** and the cyclopropanation product relative to the natural product analog (**4′**). However, in terms of our purpose, this small shift in preference is acceptable.

The bifurcating pathway in Scheme 3 was described previously by Hong and Tantillo.[8] The intrinsic reaction

coordinate (IRC)[50,51] from TS $2^{\ddagger}$ goes directly to the natural product cation **4**. TS $3^{\ddagger}$ is very similar to a structure located along this IRC. IRC calculations starting from TS $3^{\ddagger}$ lead to cations **4** and **5**.

Computational Details of the Direct Dynamics Simulations. The direct dynamics simulations were performed with VENUS05[52−54] coupled to NWChem.[29,30] The initial conditions were chosen from 330.15 K Boltzmann distributions for reaction coordinate translation and the vibrational and three rotational degrees of freedom.[55] This model for initiating trajectories assumes that recrossing of the TS is unimportant,[56] so that TST gives an accurate rate constant for the **1** → **4** + **5** reaction. The trajectories were initiated at TS $2^{\ddagger}$ and directed randomly toward either reaction products or **1**. Quasiclassical sampling,[55] which includes ZPE, was used to randomly select vibrational states for the initial conditions. The normal-mode energies for the vibrational states were transformed to the Cartesian coordinates and velocities used for calculating the direct dynamics trajectories by choosing a random classical phase for each normal mode. Recent work has shown that this approach for TS sampling leads to the same dynamics as using the Wigner distribution to transform the normal-mode energies to coordinates and momenta.[57] An ensemble of 110 trajectories was computed, which provided statistically significant trajectory results.

With respect to the classical potential energy of TS $2^{\ddagger}$, the average total energy of the trajectories is the ZPE of $2^{\ddagger}$, the thermal energy for the vibrational modes of $2^{\ddagger}$, and the average reaction coordinate and external rotational energies RT and $3RT/2$; i.e.

$$\begin{aligned}\langle E_{\text{total}}\rangle &= \text{ZPE} + \langle E_{\text{vib}}(T)\rangle + RT + 3RT/2 \\ &= 320.2\ \text{kcal/mol} \end{aligned} \quad (1)$$

where T = 330.15 K. The average E_{total} of the 110 selected trajectories is 320.5 kcal/mol and nearly the same as the above statistical thermodynamic value, which illustrates that the ensemble of trajectories is sufficiently large to give an average energy nearly the same as the statistical thermodynamic value. The average value of the rotational quantum number J for the initial conditions of all 110 trajectories is 175.

The trajectories were propagated for 1 ps using the velocity-Verlet integration scheme[58] with 0.5 fs time steps. Compared to the mean average total energy of 320.5 kcal/mol, the mean average energy variation for the velocity Verlet integrator after 1 ps is 1.06 kcal/mol. Integrating 1 ps took 32 h of computer time running on five dual 2.67 GHz X5650 six-core nodes (a total of 60 cores) with DDR InfiniBand interconnect.

Convergence criteria for the electronic structure portion of the direct dynamics were modified. For self-consistent field (SCF) calculations, the norm of the orbital gradient (convergence threshold, keyword THRESH) was tightened to 1.0×10^{-5} (default = 1.0×10^{-4}). The corresponding SCF integral screening threshold (keyword TOL2E) was loosened to 1.0×10^{-12} (default = 1.0×10^{-14}). The DFT convergence of total energy (keyword ENERGY) was tightened to 1.0×10^{-7} (default = 1.0×10^{-6}), and the convergence of the orbital gradient (keyword GRADIENT) was tightened to 1.0×10^{-5} (default = 5.0×10^{-4}).

PES and RRKM Rate Constant for Unimolecular Ring-Opening Reactions of the Pimaradienyl Cation. As discussed in the next section, a significant fraction of the trajectories initiated at TS $2^{\ddagger}$, and directed toward the pimaradienyl cation **1**, did not remain as **1** but underwent ring-opening reactions to **7** and **8** (see Scheme 5). The relative classical potential energies for these species are listed in Table 3. Included in parentheses are the relative energies with ZPE corrections scaled by 0.9806.[35]

Scheme 5. Detailed Mechanism for the Ring-Opening Reactions Observed Converting Pimaradienyl Cation 1 to Cations 7 and 8

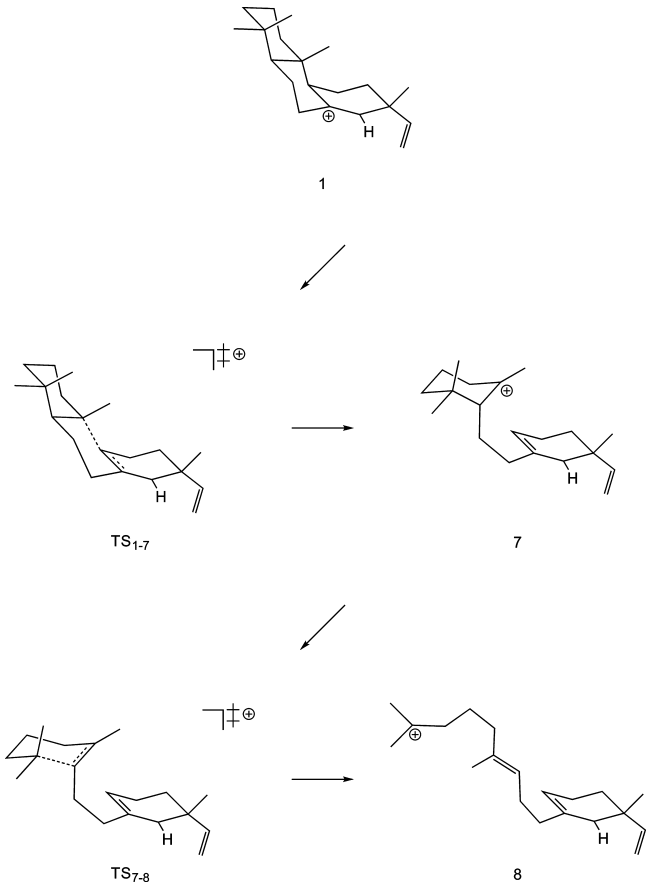

Table 3. Relative Potential Energies for Stationary Points on the PES for Ring-Opening Reactions of the Pimaradienyl Cation[a]

stationary point[b]	V [kcal/mol]
1	0.00 (*0.00*)
$\mathbf{TS}_{1-7}$	11.81 (*9.51*)
7	11.51 (*9.24*)
$\mathbf{TS}_{7-8}$	30.69 (*25.34*)
8	25.10 (*19.78*)

[a]Relative energies are B3LYP/6-31G(d) classical potential energies, without ZPE (normal text) and with scaled ZPE (*underlined italics*). [b]The stationary points are identified in Scheme 5.

As shown in Table 3, the potential energies of **7** and **8** are substantially higher than that of **1**, and it is of interest if the formations of **7** and **8** in the trajectory simulation are consistent with a statistical model of the chemical dynamics. To address this question, a qualitative analysis of the **1**→**7**, **7**→**1**, **7**→**8**, and **8**→**7** unimolecular rate constants was made by calculating them using RRKM theory[59,60] with all internal degrees of freedom

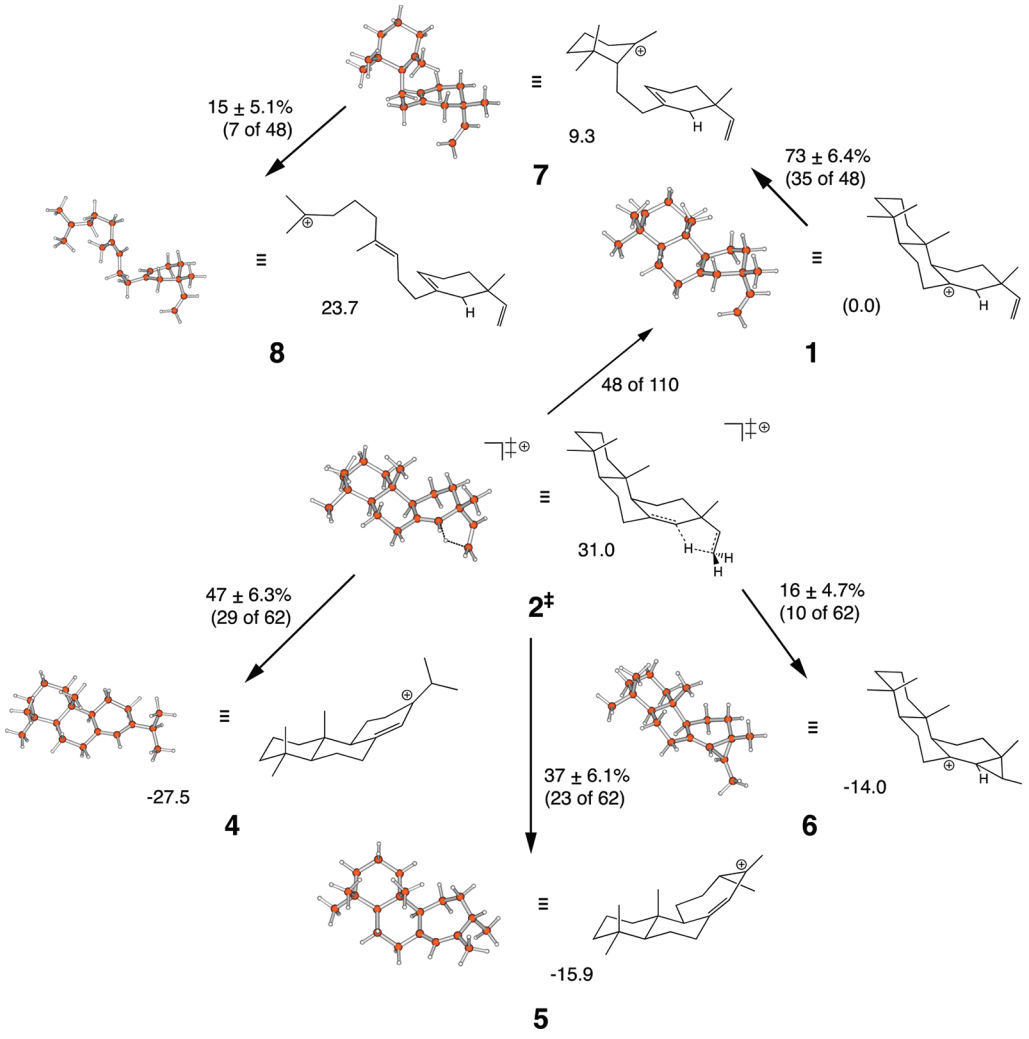

Figure 2. Summary of the results for the 110 randomly selected trajectories utilizing B3LYP/6-31G(d) forces. Of these, 62 proceeded toward products and 48 toward the reactant.

treated as harmonic oscillators. To illustrate, for the classical RRKM calculation, the energy of **1** is 354.2 kcal/mol and the **1**→**7** unimolecular barrier is 11.8 kcal/mol. The classical RRKM rate constant ratios are **1**→**7**/**7**→**1** = 5.88 ps^{-1}/0.82 ps^{-1} and **7**→**8**/**8**→**7** = 5.42 ps^{-1}/1.85 ps^{-1}. The classical RRKM **1**→**7** lifetime is 0.17 ps, and this calculation predicts that a substantial amount of **7** should be formed during the 1 ps of the trajectory integration.

The first-order differential equations connecting **1**, **7**, and **8** may be numerically integrated to determine the amounts of **1**, **7**, and **8** versus time. The classical RRKM rate constants give a **1**/**7**/**8** ratio of 1.0:6.4:17.9 when the trajectories are halted at 1 ps. The long-time steady-state equilibrium ratio is 1.0:7.4:21.6. There is only a small difference between the 1 ps and long-time ratios, and thus, the RRKM equilibrium conditions are nearly reached at 1 ps.

The origin of the much larger **1**→**7** rate constant as compared to that for **7**→**1** is the "looseness" of **7** with much lower vibrational frequencies as compared to **1**, which results in a higher density of states for **7**. At low energies for **1**, the **1**→**7** rate constant is larger than that for **7**→**1**, but the difference decreases as the energy is increased. When the energy of **1** reaches 253 kcal/mol, the rate constant ratio for **1**→**7**/**7**→**1** becomes unity.

The above classical RRKM calculation assumes that the ZPE for the initial condition of TS $\mathbf{2}^{\ddagger}$ is distributed randomly between the vibrational modes of **1**, **7**, and **8**. At short times, the classical intramolecular dynamics may be approximately vibrationally adiabatic,[3,61] with ZPE not flowing freely. For such dynamics, a quantum RRKM calculation may be more appropriate. For this calculation, the energy of **1** is 46.1 kcal/mol, and the **1**→**7** threshold is 9.5 kcal/mol.[62] The quantum harmonic RRKM rate constant ratios are **1**→**7**/**7**→**1** = 0.0397 ps^{-1}/0.665 ps^{-1} and **7**→**8**/**8**→**7** = 0.439 × 10^{-4} ps^{-1}/0.018 ps^{-1}. At the 1 ps conclusion of the trajectories, these rate constants give a **1**/**7**/**8** ratio of 33.1:1.0:<0.01. The long-time ratio is 16.8:1.0:<0.01. As for the above classical RRKM calculations, the 1 ps and long-time ratios are similar. However, in contrast to the classical calculation, the quantum calculation predicts most of the trajectories to remain as **1** and not form **7** and **8**.

RESULTS AND DISCUSSION

Product Yield and Reaction Pathways. The chemical species formed by the 110 trajectories run with B3LYP/6-31G(d) forces are summarized in Figure 2. A total of 62 trajectories propagate toward products; of these, 47 ± 6.3% form **4**, while 37 ± 6.1% form **5**. This corresponds to a relative

dx.doi.org/10.1021/ct300037p | J. Chem. Theory Comput. 2012, 8, 1212−1222

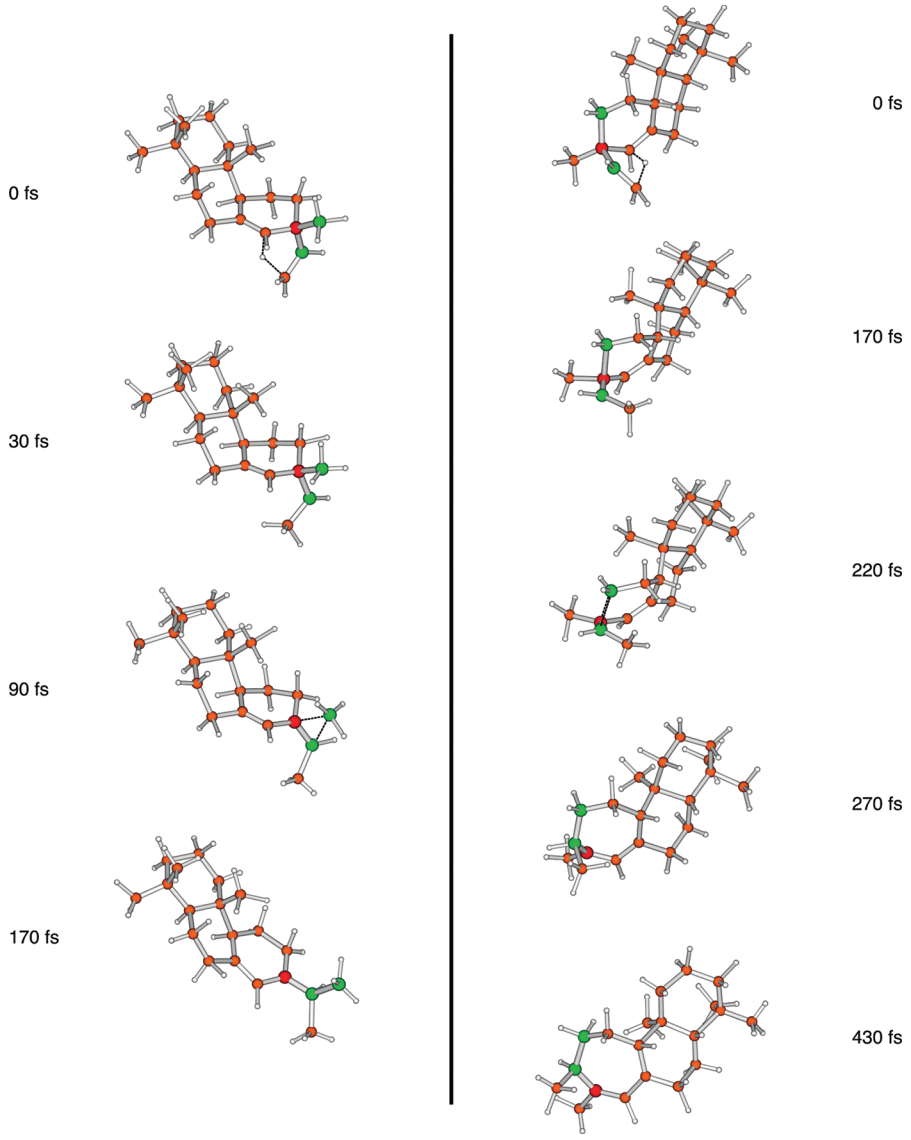

Figure 3. Snapshots of example trajectories forming products **4** (left) and **5** (right). Carbon atoms that break/form bonds are color-coded such that a C_{red}−C_{green} bond will break and a C_{green}−C_{green} bond will form.

4/**5** ratio of 1.3:1. This ratio is remarkable when we are reminded that **5** is not observed in nature. It is also important to note that this ratio is in line with those that we presented earlier for the truncated C_{10} system, in which we varied both the model chemistry (i.e., B3LYP and MP2 with the 6-31+G(d,p) basis set, for which **4′**/**5′** is 1.6:1 and 2.0:1, respectively)[1] and basis set as described above for which **4′**/**5′** is 1.1:1 for B3LYP with the 6-31G(d) basis set. Additionally, for the current study, the cyclopropanated product **6** is formed 16 ± 4.7% of the time. On the basis of the results presented above, this ratio of **6** is likely overestimated, although qualitatively similar. It is important to note that natural products have been isolated from *Caesalpinia mimosoides* (mimosol D),[63] *C. pulcherrima*,[64] and *Myrospermum frutescens* (chagresnone)[65,66] with the same carbon skeleton as **6**, albeit oxidized.

Forty-eight of the trajectories moved toward the pimaradienyl cation (**1**), and all initially formed this species. However, this chemical system has sufficient energy to undergo further reaction pathways, which were not available for the truncated C_{10} system. A large fraction of **1** (73 ± 6.41%, 35 of 48) underwent a C−C bond breaking event (defined by occurrence of a structure with a C−C contact greater than 2.0 Å), resulting in a new tertiary carbocation center and a newly formed C═C double bond, yielding **7** (Figure 2). This bond-breaking event is aided by the hyperconjugation of the carbocationic center with two of the parallel C−C bonds of the cyclohexane ring. Furthermore, seven of the 35 trajectories that formed **7** underwent a second C−C bond rupture forming **8** with a tertiary carbocationic center.

The **1**/**7**/**8** ratio at 1 ps from the trajectories is 1.0:2.2:0.5 in comparison to the respective classical and quantum RRKM ratios of 1.0:6.4:17.9 and 33.1:1.0:<0.01. The trajectory ratio is intermediate to the classical and quantum RRKM ratios. Compared to classical RRKM, the trajectory ratio has more of **1** and **7** dominating instead of **8**. This result suggests that there is a degree of vibrational adiabaticity in the initial unimolecular dynamics of **1**, **7**, and **8**.

The experimental long-time, fixed-energy equilibrium **1**:**7**:**8** ratio is given by quantum RRKM theory with accurate anharmonic corrections in calculating the densities of state for **1**, **7**, and **8**. The above harmonic quantum RRKM calculation results in a negligible yield of **8** and only 6% of

these species existing as **7**. It will be of interest, in future work, to see if this finding is maintained when accurate anharmonic corrections are included in the density of states. However, obtaining these corrections will be a difficult task. If the formations of **7** and **8** are found to be important for the gas-phase dynamics without the enzyme, their formation undoes much of the work done by the enzyme and, hence, must be repressed by abietadiene synthase.

Atomic-Level Reaction Mechanisms. Figure 3 shows snapshots along example trajectories forming products **4** and **5**. Formation of the abietadienyl cation (**4**) occurs relatively quickly, with C−H bond formation completed by 45 fs (σ = 30) on average and C−C bond formation completed by 175 fs (σ = 54) on average.[67] These times are approximately the same as those for the C_{10} system where C−H bond formation was complete by 44 fs (σ = 33), and C−C bond formation was complete by 191 fs (σ = 82), on average.[1] Formation of **5** occurs through C−H bond formation on a similar time scale (average = 44 fs, σ = 35); however, the C−C bond-forming event takes significantly longer with an average time of 255 fs (σ = 55).[67] The reaction time (measured as the time to complete C−C bond formation)[67] for all trajectories forming **4** and **5** are displayed in Figure 4. Again, these times are approximately the same as those for the C_{10} system where C−H bond formation was complete by 37 fs (σ = 24), and C−C bond formation was complete by 272 fs (σ = 115), on average.[1]

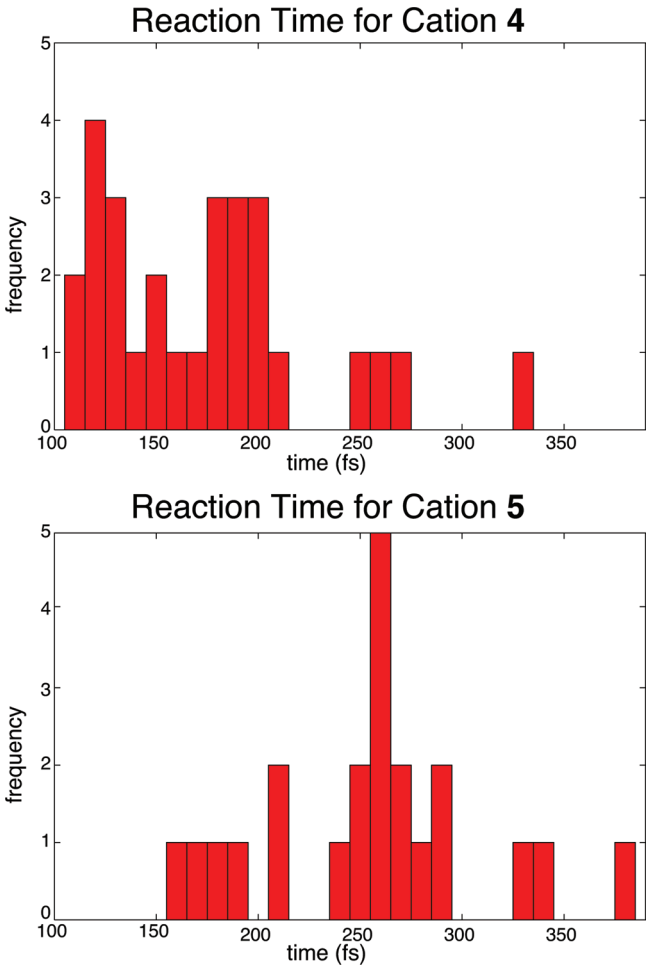

Figure 4. Distribution plots (histograms) for the time for reaction completion forming products **4** (top) and **5** (bottom). Bin size is 10 fs.

On the whole, the distribution plot for **4** has a shape tailing off at longer times while that for **5** has a bell shape. This is in contrast to the C_{10} system where distribution plots for both **4′** and **5′** tail off at longer times much as **4** does here.[1]

As a measure of the synchronicity of the C−H and C−C bond forming events (or lack thereof),[68] the time gap between these events[69] was computed, and the resulting distribution plots are in Figure 5. On average, the time gap between these

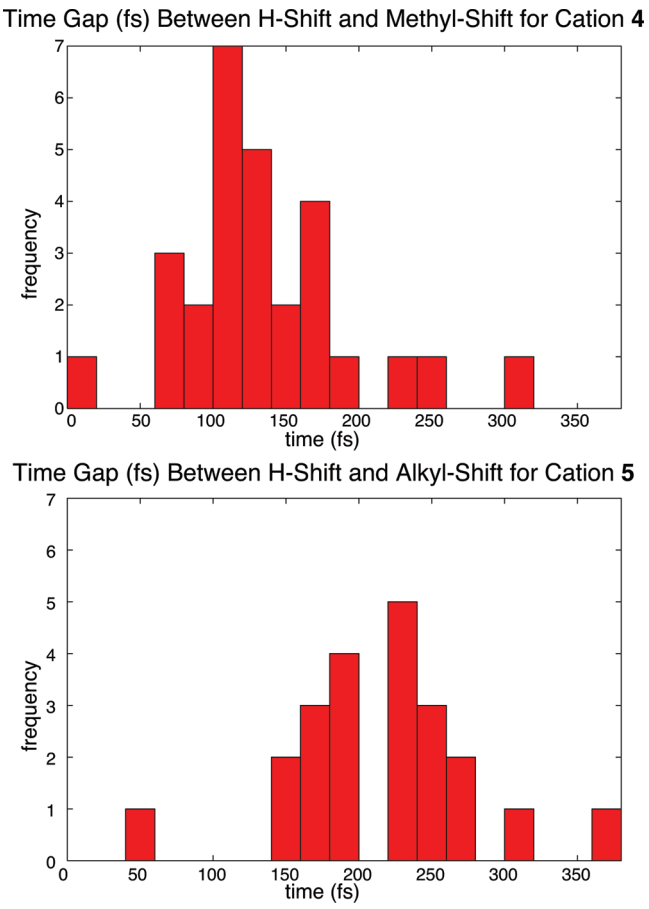

Figure 5. Distribution plots (histograms) for the time gap[69] between C−H and C−C bond-forming events[67] in the generation of **4** (top) and **5** (bottom). Bin size is 20 fs.

events is 130 fs (σ = 60) for the formation of **4** and 211 fs (σ = 64) when forming **5**. These are found to be very similar to those of **4′** (147 fs, σ = 89) and **5′** (235 fs, σ = 113).

Figure 6 shows snapshots along a sample trajectory forming product **6**. This reaction starts with a C−H bond shift concluding on the same time scale as for **4** and **5** formation (average = 46 fs, σ = 28). Carbon−carbon bond formation takes, on average, 200 fs (σ = 134). In the C_{10} system, we found that C−H bond formation occurs on a similar time scale (54 fs, σ = 38).[1] However, the C−C bond formation takes significantly less time in the C_{10} system (112 fs, σ = 16).[1] This difference in time may be attributable to additional relaxation time in the fused ring system present in our C_{20} molecule, but not in our C_{10} model. Note that thermodynamic considerations of the Bell−Evans−Polanyi variety would dictate that, all else being equal, the barrier to form **6** should be lower than that to form the C_{10} analog (relative energies: **6** = −14.0 kcal/mol, C_{10} analog = −0.03 kcal/mol).[1,70,71] Also of note is the substantial vibrational energy localized in the C−C bonds of the

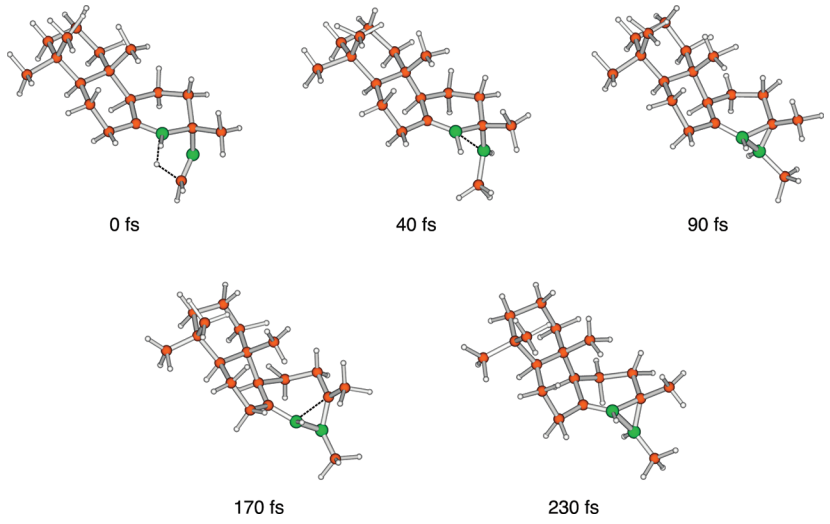

Figure 6. Snapshots of an example trajectory forming product **6**. Carbon atoms that break/form bonds are color coded such that a C_{red}–C_{green} bond will break and a C_{green}–C_{green} bond will form.

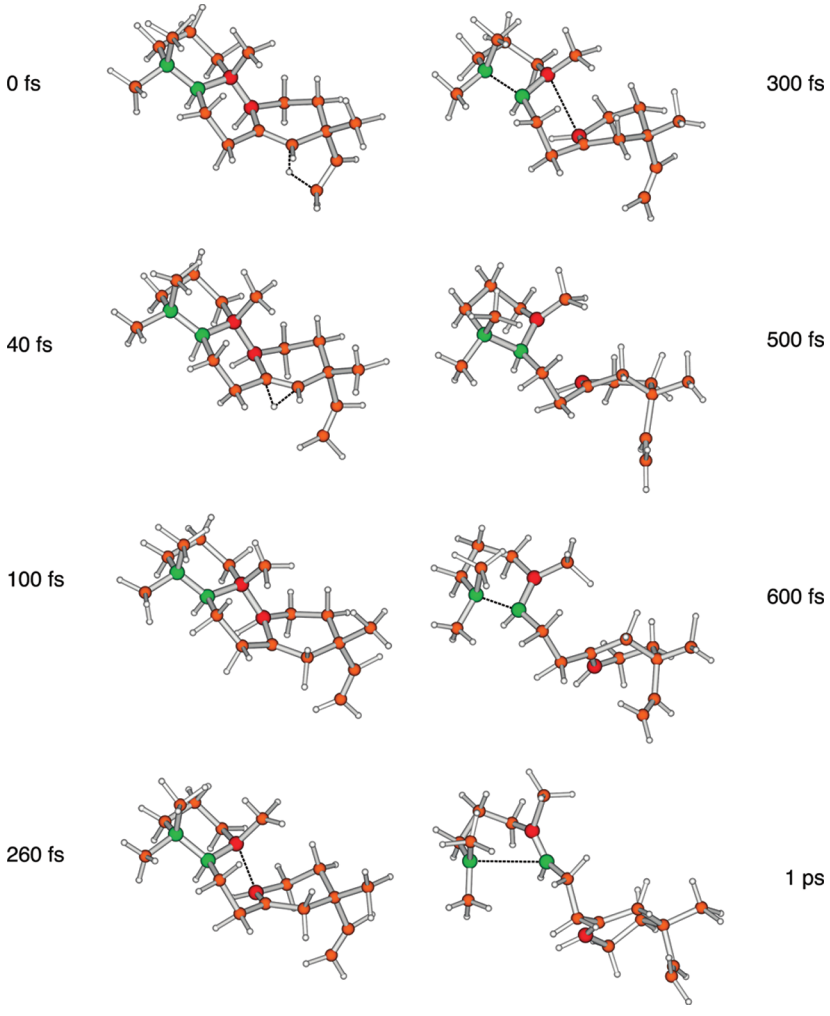

Figure 7. Snapshots of an example trajectory forming **8**. Carbon atoms that break bonds are color coded such that the C_{red}–C_{red} and C_{green}–C_{green} bonds will break.

cyclopropane ring, as can be seen in the 170 fs snapshot. This localization of energy was noted in the C_{10} system as well.[1]

Figure 7 shows snapshots for a representative trajectory that ultimately ends up breaking open two cyclohexane rings and ends at **8**. The trajectory initially moves toward **1**. Along this pathway, the H atom shifts back, and its momentum (along with hyperconjugation) carries it toward the formal carbocationic center (40 fs snapshot). The carbocationic center then

dx.doi.org/10.1021/ct300037p | J. Chem. Theory Comput. 2012, 8, 1212–1222

aligns its empty p orbital with parallel C−C σ bonds of the adjacent cyclohexane ring (110, 260 fs snapshots). One of the C−C bonds breaks preferentially resulting in a tertiary carbocation and the formation of **7**. In total, 73% of trajectories sent toward **1** break this C−C bond, forming **7**, and it takes an average of 465 fs (σ = 249) from the time the trajectory is initiated at the TS.

The representative trajectory in Figure 7 continues to rearrange by aligning the newly generated carbocationic center with the parallel C−C bonds of the next cyclohexane ring (see 500, 600 fs snapshots), resulting in **8**. Only 7 of the 48 trajectories (15%) sent toward **1** break this second C−C bond. On average, this second C−C bond-breaking event occurs at 726 fs (σ = 152).

CONCLUSION

In this report, we have shown how trajectories traverse the PES for the pimaradienyl cation → abietadienyl cation rearrangement. This is the only biosynthetically relevant chemical reaction shown to have a PES with a pathway bifurcation. The reaction pathway for the above rearrangement has a bifurcation, in the absence of an enzyme, leading to cation **5**, a precursor to as of yet unobserved diterpenoid natural products, in addition to abietadienyl cation **4**, precursor to known abietadiene terpenoids. The B3LYP/6-31G(d) direct dynamics simulations give a **4**/**5** ratio of ∼1.3:1. This ratio is in line with our findings for the truncated C_{10} system, for which we varied many key features (including model chemistry[1] and basis set; *vide supra*). In addition to **5**, the pimaradienyl cation → abietadienyl cation rearrangement also leads to cyclopropylcarbinyl cation **6** (although our simulations slightly overestimate the ratio), a carbon skeleton whose oxidized form is present in several isolated natural products.[63−66]

Previous comparisons[3,72−74] of classical chemical dynamics simulations with experimental results and quantum dynamics indicate that the classical dynamics give accurate results for short-time post-transition state dynamics in moving from a high energy TS to products. This is the nature of the dynamics observed here in moving directly from TS **2**‡ to the products **4**, **5**, and **6**, without intermediate formation. In contrast, the applicability of classical dynamics for the **1** ⇌ **7** ⇌ **8** unimolecular reactions is more uncertain. Though classical dynamics may approximately conserve ZPE motions for short times,[3] if the classical dynamics is ergodic then the ZPE flows freely at long times.[75] Thus, classical dynamics may allow trajectories to cross a TS without ZPE in the necessary modes (those orthogonal to the reaction coordinate).[75] The long-time equilibrium, constant-energy ratio of **1**, **7**, and **8** is given by RRKM theory. A harmonic model approximates this ratio, and classical harmonic RRKM theory, which assumes free flow of ZPE, gives a long-time **1**/**7**/**8** ratio of 1.0:6.4:17.9. In contrast, quantum harmonic RRKM theory gives a **1**/**7** ratio of 16.8:1.0 with negligible **8**. The free flow of ZPE has a pronounced effect on the equilibrium distribution of **1**, **7**, and **8**.

The simulations show that trajectories initiated at the TS connecting the pimaradienyl and abietadienyl cations, and directed toward the former, form not only this species but also cations **7** and **8** (through further intramolecular fragmentation). When the trajectories were halted after 1.0 ps of motion, the **1**/**7**/**8** ratio was 1.0:2.2:0.5. As discussed above, it is possible that the trajectory simulation does not provide an accurate **1**/**7**/**8** ratio as a result of the unphysical flow of ZPE. The long-time, equilibrium ratio is given by RRKM theory, and at the quantum harmonic level, the **1**/**7** ratio is 16.8:1.0 with negligible **8**. Thus, at the harmonic level, quantum RRKM theory predicts that, in contrast to the trajectory result, unimolecular decomposition of **1** to **7** and **8** is unimportant. However, the harmonic model may be an inaccurate representation of the anharmonic densities of state for **1**, **7**, and **8**, and it is possible that the classical unimolecular dynamics for **1** ⇌ **7** ⇌ **8** within 1 ps, on the anharmonic PES, are more accurate than the prediction of harmonic quantum RRKM theory.

The above discussion pertains to the chemical dynamics for the B3LYP/6-31G(d) PES used for the simulations. It is possible that this level of theory underestimates the barriers for formation of **7** and **8** from **1**.[46−48] If this is the case, the trajectories may give negligible **7** and **8** even with the unphysical flow of ZPE.

If **7** and **8** are formed from **1** in the absence of the enzyme then, in nature, abietadiene synthase must suppress reaction to not only **5** and **6** but also **7** and **8**. This may be done through selective steric interactions, C−H/π[76−78] or cation/π[79−81] interactions. We continue to investigate this reaction, with interests turned toward the effect solvent plays on this PES as well as inclusion of an enzyme model.

ASSOCIATED CONTENT

Supporting Information

Coordinates and energies for optimized structures. This material is available free of charge via the Internet at http://pubs.acs.org.

AUTHOR INFORMATION

Corresponding Author

*E-mail: bill.hase@ttu.edu.

Notes

The authors declare no competing financial interest.

ACKNOWLEDGMENTS

This material is based upon work supported by the National Science Foundation under Grant Nos. CHE-0957521, CHE-0957416, and TG-CHE-110010 (TeraGrid) and the Robert A. Welch Foundation under Grant No. D-0005. Support was also provided by the High Performance Computing Center (HPCC) at Texas Tech University (TTU), under the direction of Philip W. Smith, the Texas Advanced Computing Center (TACC) of the University of Texas at Austin, and the TTU Department of Chemistry & Biochemistry cluster Robinson, whose purchase was funded by the National Science Foundation under the CRIF-MU Grant No. CHE-0840493. Furthermore, we thank Dan Ferguson (TTU) for helpful discussion and comments regarding the direct dynamics and HPCC software.

REFERENCES

(1) Siebert, M. R.; Zhang, J.; Addepalli, S. V.; Tantillo, D. J.; Hase, W. L. *J. Am. Chem. Soc.* **2011**, *133*, 8335−8343.
(2) Ess, D. H.; Wheeler, S. E.; Iafe, R. G.; Xu, L.; Çelebi-Ölçüm, N.; Houk, K. N. *Angew. Chem., Int. Ed.* **2008**, *47*, 7592−7601.
(3) Lourderaj, U.; Park, K.; Hase, W. L. *Int. Rev. J. Phys. Chem.* **2008**, *27*, 361−403.
(4) Thomas, J. B.; Waas, J. R.; Harmata, M.; Singleton, D. A. *J. Am. Chem. Soc.* **2008**, *130*, 14544−14555.
(5) Hamaguchi, M.; Nakishi, M.; Nagai, T.; Nakamura, T.; Abe, M. *J. Am. Chem. Soc.* **2007**, *129*, 12981−12988.

(6) Singleton, D. A.; Hang, C.; Szymanski, M. J.; Meyer, M. P.; Leach, A. G.; Kuwata, K. T.; Chen, J. S.; Greer, A.; Foote, C. S.; Houk, K. N. *J. Am. Chem. Soc.* **2003**, *125*, 1319−1328.
(7) Wales, D. J. *J. Chem. Phys.* **2000**, *113*, 3926−3927.
(8) Hong, Y. J.; Tantillo, D. J. *Nature Chem.* **2009**, *1*, 384−389.
(9) Ramquet, M.-N.; Dive, G.; Deharent, D. *J. Chem. Phys.* **2000**, *112*, 4923−4934.
(10) González-Lafont, À; Moreno, M.; Lluch, J. M. *J. Am. Chem. Soc.* **2004**, *126*, 13089−13094.
(11) Valtazanos, P.; Ruedenberg, K. *Theor. Chim. Acta* **1986**, *69*, 281−307.
(12) Taketsugu, T.; Tajima, N.; Hirao, K. *J. Chem. Phys.* **1996**, *105*, 1933−1939.
(13) Kumeda, Y.; Taketsugu, T. *J. Chem. Phys.* **2000**, *113*, 477−484.
(14) Lasorne, B.; Dive, G.; Desouter-Lecomte, M. *J. Chem. Phys.* **2003**, *118*, 5831−5840.
(15) Colwell, S. M. *Mol. Phys.* **1984**, *51*, 1217−1233.
(16) Colwell, S. M.; Handy, N. C. *J. Chem. Phys.* **1985**, *82*, 1281−1290.
(17) Baker, J.; Gill, P. M. W. *J. Comput. Chem.* **1988**, *9*, 465−475.
(18) Yanai, T.; Taketsugu, T.; Hirao, K. *J. Chem. Phys.* **1997**, *107*, 1137−1146.
(19) Castaño, O.; Frutos, L. −M.; Palmeiro, R.; Notario, R.; Andrés, J. −L.; Gomperts, R.; Blancafort, L.; Robb, M. A. *Angew. Chem., Int. Ed.* **2000**, *39*, 2095−2097.
(20) Hrovat, D. A.; Borden, W. T. *J. Am. Chem. Soc.* **1992**, *114*, 5879−5881.
(21) Wenthold, P. G.; Hrovat, D. A.; Borden, W. T.; Lineberger, W. C. *Science* **1996**, *272*, 1456−1459.
(22) Castaño, O.; Palmeiro, R.; Frutos, L. M.; Luisandrés, J. *J. Comput. Chem.* **2002**, *23*, 732−736.
(23) Debbert, S. L.; Carpenter, B. K.; Hrovat, D. A.; Borden, W. T. *J. Am. Chem. Soc.* **2002**, *124*, 7896−7897.
(24) Hrovat, D. A.; Duncan, J. A.; Borden, W. T. *J. Am. Chem. Soc.* **1999**, *121*, 169−175.
(25) Roth, W. R.; Wollweber, D.; Offerhas, R.; Rekowski, V.; Lennartz, H. W.; Sustmann, R.; Müller, W. *Chem. Ber.* **1993**, *126*, 2701−2715.
(26) Bartsch, R. A.; Chae, Y. M.; Ham, S.; Birney, D. M. *J. Am. Chem. Soc.* **2001**, *123*, 7479−7486.
(27) Phillips, M. A.; Croteau, R. B. *Trends Plant Sci.* **1999**, *4*, 184−190.
(28) McCoy, M. *Chem. Eng. News* **2000**, *78*, 13−15.
(29) Bylaska, E. J.; de Jong, W. A.; Govind, N.; Kowalski, K.; Straatsma, T. P.; Valiev, M.; Wang, D.; Apra, E.; Windus, T. L.; Hammond, J.; Nichols, P.; et al. *NWChem, A Computational Chemistry Package for Parallel Computers*, version 5.1; Pacific Northwest National Laboratory: Richland, WA, 2007.
(30) Kendall, R. A.; Apra, E.; Bernholdt, D. E.; Bylaska, E. J.; Dupuis, M.; Fann, G. I.; Harrison, R. J.; Ju, J.; Nichols, J. A.; Nieplocha, J.; Straatsma, T. P.; Windus, T. L.; Wong, A. T. *Comput. Phys. Commun.* **2000**, *128*, 260−283.
(31) Becke, A. D. *J. Chem. Phys.* **1993**, *98*, 5648−5652.
(32) Becke, A. D. *J. Chem. Phys.* **1993**, *98*, 1372−1377.
(33) Lee, C.; Yang, W.; Parr, R. G. *Phys. Rev. B: Solid State* **1988**, *37*, 785−789.
(34) Stevens, P. J.; Devlin, F. J.; Chabalowski, C. F.; Frisch, M. J. *J. Phys. Chem.* **1994**, *98*, 11623−11627.
(35) Scott, A. P.; Radom, L. *J. Phys. Chem.* **1996**, *100*, 16502−16513.
(36) Woodcock, H. L.; Schaefer, H. F.; Schreiner, P. R. *J. Phys. Chem. A* **2002**, *106*, 11923−11931.
(37) Tsuzuki, S.; Lüthi, H. P. *J. Chem. Phys.* **2001**, *114*, 3949−3957.
(38) Schreiner, P. R.; Fokin, A. A.; Pascal, R. A. Jr.; de Meijera, A. *Org. Lett.* **2006**, *8*, 3635−3638.
(39) Check, C. E.; Gilbert, T. M. *J. Org. Chem.* **2005**, *70*, 9828−9834.
(40) Redfern, P. C.; Zapol, P.; Curtiss, L. A.; Raghavachari, K. *J. Phys. Chem. A* **2000**, *104*, 5850−5854.
(41) Wodrich, M. D.; Wannere, C. S.; Mp, Y.; Jarowski, P. D.; Houk, K. N.; Schleyer, P. v. R. *Chem.—Eur. J.* **2007**, *13*, 7731−7744.
(42) Grimme, S. *Angew. Chem., Int. Ed.* **2006**, *45*, 4460−4464.
(43) Wodrich, M. D.; Corminboeuf, C.; Schleyer, P. v. R. *Org. Lett.* **2006**, *8*, 3631−3634.
(44) Kang, J. K.; Musgrave, C. B. *J. Chem. Phys.* **2001**, *115*, 11040−11051.
(45) Lynch, B. J.; Fast, P. L.; Harris, M.; Truhlar, D. G. *J. Phys. Chem. A* **2000**, *104*, 4811−4815.
(46) Zhao, Y.; Tishchenko, O.; Truhlar, D. G. *J. Phys. Chem. B* **2005**, *109*, 19046−19051.
(47) Zhao, Y.; Truhlar, D. G. *Acc. Chem. Res.* **2008**, *41*, 157−167.
(48) Zhang, I. Y.; Wu, J.; Xu, X. *Chem. Commun.* **2010**, *46*, 3057−3070.
(49) Zheng, J.; Zhao, Y.; Truhlar, D. G. *J. Chem. Theory Comput.* **2007**, *3*, 569−582.
(50) Fukui, K. *Acc. Chem. Res.* **1981**, *14*, 363−368.
(51) Gonzalez, C.; Schlegel, H. B. *J. Phys. Chem.* **1990**, *94*, 5523−5527.
(52) Hase, W. L.; Bolton, K.; Sainte Claire, P. d.; Duchovic, R. J.; Hu, X.; Komornicki, A.; Li, G.; Lim, K. F.; Lu, D.-h.; Peslherbe, G. H.; Song, K.; Swamy, K. N.; Vande Linde, S. R.; Varandas, A.; Wang, H.; Wolf, R. J. *Venus05 − a general chemical dynamics computer program*; 2004.
(53) Hase, W. L.; Duchovic, R. J.; Hu, X.; Komornicki, A.; Lim, K. F.; Lu, D. H.; Peslherbe, G. H.; Swamy, K. N.; Vande Linde, S. R.; Varandas, A.; Wang, H.; Wolf, R. J. *Quant. Chem. Prog. Exch. Bull.* **1996**, *16*, 671.
(54) Hu, X.; Hase, W. L.; Pirraglia, T. *J. Comput. Chem.* **1991**, *12*, 1014−1024.
(55) Peslherbe, G. H.; Wang, H.; Hase, W. L. *Adv. Chem. Phys.* **1999**, *105*, 171−201.
(56) Gonzalez-James, O. M.; Kwan, E. E.; Singleton, D. A. *J. Am. Chem. Soc.* **2012**, *134*, 1914−1917.
(57) Sun, L.; Hase, W. L. *J. Chem. Phys.* **2010**, *133*, 034027.
(58) Swope, W. C.; Anderson, H. C.; Berens, P. H.; Wilson, K. R. *J. Chem. Phys.* **1982**, *76*, 637−649.
(59) Baer, T.; Hase, W. L. *Unimolecular Reaction Dynamics. Theory and Experiments*, Oxford University Press: New York, 2006.
(60) Zhu, L.; Hase, W. L. *QCPE Bull.* **1994**, *14*, 644.
(61) Marcus, R. A. *J. Phys. Chem.* **1979**, *83*, 204−207.
(62) Vayner, G.; Addepalli, S. A.; Song, K.; Hase, W. L. *J. Chem. Phys.* **2006**, *125*, 014317.
(63) Yodsaoue, O.; Karalai, C.; Ponglimanont, C.; Tewtrakul, S.; Chantrapromma, S. *Phytochemistry* **2010**, *71*, 1756−1764.
(64) Yodsaoue, O.; Karalai, C.; Ponglimanont, C.; Tewtrakul, S.; Chantrapromma, S. *Tetrahedron* **2011**, *67*, 6838−6846.
(65) Torres-Mendoza, D.; González, L. D. U.; Ortega-Barría, E.; Coley, P. D.; Kursar, T. A.; Capson, T. L.; McPhail, K.; Cubilla-Rios, L. *J. Nat. Prod.* **2004**, *67*, 1711−1715.
(66) Torres-Mendoza, D.; González, L. D. U.; Ortega-Barría, E.; Coley, P. D.; Kursar, T. A.; Capson, T. L.; McPhail, K.; Cubilla-Rios, L. *J. Nat. Prod.* **2006**, *69*, 1256.
(67) Each event was deemed complete at the first time that the interatomic distance in question fell below the distance for the equilibrium structure: For **4**, key equilibrium interatomic distances are 1.094 and 1.562 Å for the C−H and C−C bonds, respectively. For **5**, these distances are 1.093 and 1.537 Å for the C−H and C−C bonds, respectively, and for **6**, these distances are 1.094 and 1.636 Å for the C−H and C−C bonds, respectively. Interatomic distances were printed every 10 fs, which represents the resolution in which the stated times reside.
(68) Tantillo, D. J. *J. Phys. Org. Chem.* **2008**, *21*, 561−570.
(69) Xu, L.; Doubleday, C. E.; Houk, K. N. *J. Am. Chem. Soc.* **2010**, *132*, 3029−3037.
(70) Bell, R. P. *Proc. R. Soc. London, Ser. A* **1936**, *154*, 414−429.
(71) Evans, M. G.; Polanyi, M. *Trans. Faraday Soc.* **1938**, *34*, 11−24.
(72) Untch, A.; Schinke, R.; Cotting, R.; Huber, J. R. *J. Chem. Phys.* **1993**, *99*, 9553−9566.
(73) Dong, E.; Setser, D. W.; Hase, W. L.; Song, K. *J. Phys. Chem. A.* **2006**, *110*, 1484−1490.

(74) López, J. G.; Vayner, G.; Lourderaj, U.; Addepalli, S. V.; Kato, S.; de Jong, W. A.; Windus, T. L.; Hase, W. L. *J. Am. Chem. Soc.* **2007**, *129*, 9976−9985.
(75) Hase, W. L.; Buckowski, D. G. *J. Comput. Chem.* **1982**, *3*, 335−343.
(76) Nishio, M.; Hirota, M.; Umezawa, Y. *The CH/π Interaction: Evidence, Nature, and Consequences*; Wiley-VCH: New York, 1998.
(77) Brandl, M.; Weiss, M. S.; Jabs, A.; Sühnel, J.; Hilgenfeld, R. *J. Mol. Biol.* **2001**, *307*, 357−377.
(78) Tsuzuki, S.; Honda, K.; Uchimaru, T.; Mikami, M.; Tanabe, K. *J. Am. Chem. Soc.* **2000**, *122*, 3746−3753.
(79) Ma., J. C.; Dougherty, D. A. *Chem. Rev.* **1997**, *97*, 1303−1324.
(80) Dougherty, D. A. *Science* **1996**, *271*, 163−168.
(81) Hong, Y. J.; Tantillo, D. J. *J. Org. Chem.* **2007**, *72*, 8877−8881.